



Technical Note

A note on unsteady laminar plumes/jets

R.E. Hewitt^{a,*}, R. Bonnebaigt^b^a School of Mathematics, University of Manchester, Manchester M13 9PL, United Kingdom^b DAMTP, Wilberforce Road, Cambridge CB3 0WA, United Kingdom

ARTICLE INFO

Article history:

Received 15 November 2013

Accepted 16 November 2013

Available online 18 December 2013

Keywords:

Boundary-layer

Plume

Jet

Unsteady

Pulsatile

ABSTRACT

We consider the laminar downstream evolution of a time-varying source of momentum and buoyancy in a boundary-layer formulation. The recent work of Hewitt and Duck (2011) [5] showed that pulsatile laminar jets (in a boundary-layer model) are susceptible to a propagating wave disturbance that grows downstream. However, the work of Marzouk et al. (2003) [4] presented results for a periodic pulsatile laminar (vertical) jet with heat transfer, for which the pulsation decayed downstream. This motivates the present investigation, to examine if the thermal effects included by Marzouk et al. inhibit the growing wave phenomenon that has been found in the momentum driven case. However, in contrast to Marzouk et al., the present results demonstrate that downstream growth still exists in (vertical) laminar boundary layers when buoyancy effects are included. Our results are carefully validated against known similarity solutions in the steady case, and with both a linearised spectral decomposition for the pulsatile case and an asymptotic description of the resulting wave's spatial growth.

© 2013 Elsevier Ltd. All rights reserved.

1. Introduction and formulation

We consider the downstream evolution of an unsteady source of buoyancy and momentum in the form of a free jet/plume, which exists in an otherwise quiescent Boussinesq fluid at high Reynolds numbers. The form of the unsteadiness is a (nonlinear) pulsation superimposed onto a steady component at the source of the jet/plume. In the absence of thermal effects, the *steady* free jet has had a long history ever since its initial introduction by Schlichting [1], Bickley [2]; a well known similarity form exists that is an exact reduction of the laminar boundary-layer equations. This similarity form describes the downstream limit of any uni-directional (steady) momentum source. When the jet is extended to also include a source of buoyancy, and the momentum source is aligned with local gravity, the near-source flow is typically momentum driven, but sufficiently far downstream the evolution becomes 'plume-like', being forced by buoyancy. How quickly this transition occurs is dependent on the relative influence of momentum and buoyancy in the source conditions. Again an exact reduction of the boundary-layer system exists, which describes the far-field plume state, as presented by Brand and Lahey [3].

To address the influence of unsteady effects, the paper of Marzouk et al. [4] considers both a free and a wall jet/plume, both in the context of a laminar boundary layer system. The motivation for examining such flows is discussed at some length in their work, but here we wish to focus primarily on the conclusions and results

that were arrived at in their analysis. The jet is aligned vertically, a pulsation is introduced in the source momentum, and this source pulsation is observed to decay downstream in their numerical results. This result is somewhat at odds with the recent work on pulsation of laminar boundary-layer jets (in the absence of any buoyancy) by Hewitt and Duck [5]. This later work demonstrates that any pulsation of the source momentum (at frequency Ω) must necessarily lead to a downstream *growing* perturbation, with a growth that is proportional to:

$$\left(\frac{x^*}{Re h}\right)^{c_1} \exp\left[c_2 S^{\frac{1}{2}} Re^{-\frac{2}{3}} \left(\frac{x^*}{h}\right)^{\frac{2}{3}}\right], \quad (1)$$

in the case of a free jet (a similar result can be found for the wall jet). Here $c_{1,2}$ are known constants, x^* is the dimensional downstream coordinate, U the source velocity scale, h an initial jet width, and ν the kinematic viscosity. The dimensionless parameters are a Reynolds number, $Re = Uh/\nu$, and a Reynolds-times-Strouhal number $S = \Omega h^2/\nu$. The bulk of these asymptotic results can also be found in the work of Riley et al. [6] in the case of a free jet. This growing mode is a locally-periodic wave, with a local wave number proportional to $Re^{-\frac{1}{3}}(x^*/h)^{\frac{1}{3}}$, and a phase speed that is equal to the maximum speed of the jet. Of particular note here is that the spatial growth rate (1) remains unbounded as the dimensionless measure of pulsation frequency, S , is increased. In the high-frequency limit, the wavelength of this mode ultimately becomes comparable to the boundary layer thickness and these growing waves connect to inviscid Rayleigh modes; as mentioned by Cowley et al. [7].

* Corresponding author. Tel.: +44 1612755918.

E-mail address: richard.hewitt@manchester.ac.uk (R.E. Hewitt).

This paper is motivated by the contrasting results of Marzouk et al. [4] and Hewitt and Duck [5]. The physical difference of these two investigations lies in the inclusion of thermal effects and buoyancy. It is of some interest to investigate the effect of such forcing, to clarify if inclusion of a body force can eliminate the growing wave perturbation as the near orifice (momentum) jet develops to a larger scale (buoyant) plume. To this end, we focus attention on the vertically aligned free jet, where the influence of buoyancy is to accelerate the underlying flow, the retarding case that leads to reverse flow will not be addressed.

We begin with the two-dimensional boundary-layer equations and formulate the problem in terms of a dimensional streamfunction $\Psi^*(x^*, y^*, t^*)$ and temperature field $T^*(x^*, y^*, t^*)$. Here (x^*, y^*) is a Cartesian coordinate system, x is aligned with the streamwise direction and t^* denotes the dimensional time. At the source of the jet/plume we have a streamwise velocity scale of U , temperature of T_0 , transverse length scale h and a pulsation frequency Ω , whilst in the ambient fluid the temperature is T_∞ and density is ρ_∞ (both constants). The natural dimensionless variables are therefore introduced via: $\Psi^* = Uh\Psi(x, y, t)$, $T^* = T_\infty + T_\infty T(x, y, t)$, $y^* = yh$, $x^* = Uh^2x/v$ (giving a Reynolds number, $Re = Uh/v$, which is of course assumed to be large) and $t^* = t/\Omega$. This leads to the dimensionless governing equations in the form

$$S\Psi_{yt} + \Psi_y\Psi_{yx} - \Psi_x\Psi_{yy} = \Psi_{yyy} + \Theta, \tag{2a}$$

$$S\Theta_t + \Psi_y\Theta_x - \Psi_x\Theta_y = \frac{1}{\sigma}\Theta_{yy}, \tag{2b}$$

where (as defined above) $S = \Omega h^2/v$, and $\sigma = v/\kappa$ is a Prandtl number for a thermal diffusivity κ . The temperature measure Θ is defined as $\Theta = (g\beta T_\infty h^2)/(vU)T(x, y, t)$ where β is a coefficient of thermal expansion. This system is to be solved subject to

$$\Psi(x = 0, y, t) = \Psi_0(y, t), \quad \Theta(x = 0, y, t) = \Theta_0(y, t), \tag{2c}$$

$$\Psi_{yy}(x, y = 0, t) = 0, \quad \Theta_y(x, y = 0, t) = 0, \quad \Psi(x, y = 0, t) = 0, \tag{2d}$$

$$\Psi_y(x, y \rightarrow \infty, t) \rightarrow 0, \quad \Theta(x, y \rightarrow \infty, t) \rightarrow 0, \tag{2e}$$

$$\Psi(x, y, t = 0) = \Psi_{mit}(x, y), \quad \Theta(x, y, t = 0) = \Theta_{mit}(x, y), \tag{2f}$$

where (2d) are the appropriate symmetry conditions to be imposed along the centreline ($y = 0$) of the jet/plume.

We begin our discussion by comparing a numerical solution of (2) with the data of Marzouk et al. [4], specifically for the case presented in Fig. 8 of their paper. In terms of the formulation given above, the parameters and source conditions of Marzouk et al. [4] correspond to:

$$\Psi_0 = \begin{cases} y(1 + A \sin(t)), & \text{if } 0 \leq y \leq \frac{1}{2}, \\ \frac{1}{2}(1 + A \sin(t)), & \text{if } y > \frac{1}{2}, \end{cases} \quad \Theta_0 = \begin{cases} G_0, & \text{if } 0 \leq y \leq \frac{1}{2}, \\ 0, & \text{if } y > \frac{1}{2}, \end{cases} \tag{3a}$$

where Fig. 8 corresponds to the choices $G_0 = 5$ (being a Grashof-Reynolds number ratio), and $S = 188.5$. Increasing values of G_0 and S corresponding to higher source temperatures and higher frequencies of pulsation respectively.

Although Marzouk et al. [4] impose discontinuous (in y) source conditions, we will instead impose a smoothed version, e.g.,

$$\Theta_0 = \frac{G_0}{2} \left(1 + \tanh \left(\gamma \left(\frac{1}{2} - y \right) \right) \right), \tag{3b}$$

with a similar expression for Ψ_0 , then examine the results for increasing γ , refining the discretisation to ensure that all features are being accurately resolved.

As seen in Fig. 1(a) the steady solution ($A = 0$) is in good agreement with the results of Marzouk et al. as γ is increased. However, on the introduction of a 3% source pulsation ($A = 0.03$), the downstream development of a periodic state is significantly altered, with downstream growth being clearly visible. This downstream growth

is rapid and much less sensitive to the choice of γ than the (steady) base flow evolution. Given that our results show downstream growth of source pulsations, but those of Marzouk et al. [4] do not, we investigate this discrepancy further and take particular care to offer both numerical and analytical validation.

2. Analysis and validation of results

An investigation of a range of pulsation amplitudes A , frequencies S , scaled Grashof numbers $G_0 > 0$ and Prandtl number σ shows that downstream growth is always obtained, a result that is in agreement with the purely momentum driven jet case of Hewitt and Duck [5] and the corresponding theory of Cowley et al. [7]. This is very different behaviour than presented by Marzouk et al., but we can validate this downstream evolution in a number of respects.

Our numerical method employs the well-known Keller box scheme [8]. The method is second order in both space and time. Integration across the boundary layer and use of the boundary conditions at the axis and the far field demonstrates that the downstream heat flux

$$Q = \int_{y=0}^{\infty} \Psi_y(x, y, t)\Theta(x, y, t)dy \tag{4}$$

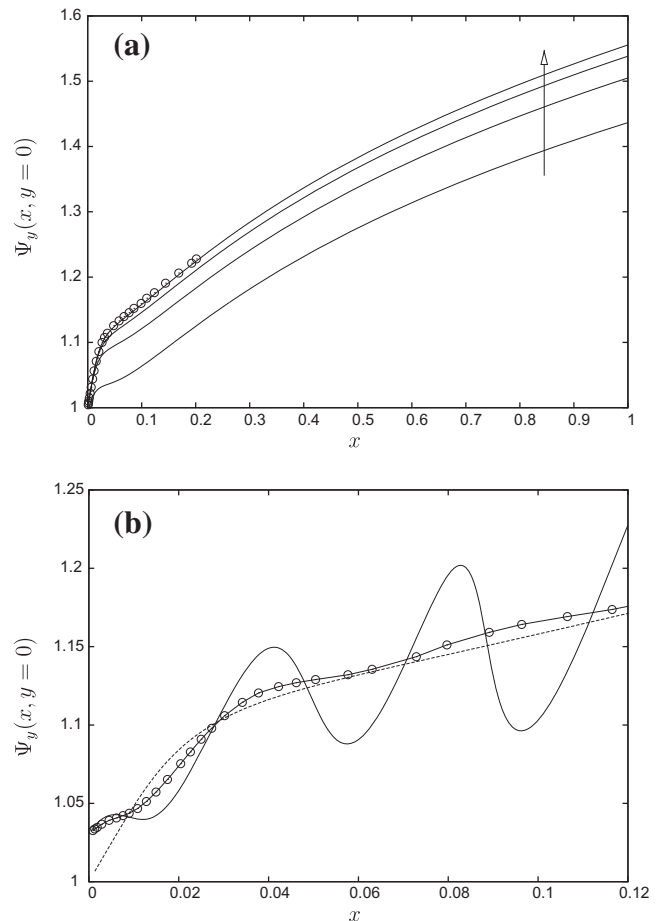


Fig. 1. (a) Solid lines show the centerline downstream velocity of steady solutions to (2) subject to (3) with $A = 0$, $G_0 = 5$, $\sigma = 0.71$ and $\gamma = 5, 10, 20, 40$ (increasing in the direction of the arrow shown), (b) The solid line shows a periodic solution of (2) subject to (3) with $A = 0.03$, $\sin(t) = 1$, $G_0 = 5$, $\sigma = 0.71$, $\gamma = 40$ and $S = 188.5$. The dashed line shows the corresponding underlying steady flow repeated from figure (a). In both cases the circular points indicate the data of [4] Fig. 8, which are in agreement for steady solutions (a) but not for unsteady solutions (b).

is conserved for a steady flow ($A = 0$). For a periodic flow, a further integration over a period $\tau = 2\pi/S$ demonstrates that the time-averaged heat flux

$$\langle Q \rangle = \tau^{-1} \int_t^{t+\tau} Q(x, t) dt \tag{5}$$

is also conserved. In both cases, as Q or $\langle Q \rangle$ is conserved at all downstream locations, it can be determined from the known steady or periodic conditions imposed at $x = 0$. Given this initial value, we can examine the maximum downstream deviation as a function of spatial and temporal resolution in the numerical scheme. In both instances the value converges quadratically with reductions in the spatial–temporal step sizes, as expected for the numerical scheme.

2.1. Low amplitude pulsation

As a further validation, an obvious approach is to examine the limit of small-amplitude source pulsation ($A \ll 1$). For small A , we can linearise by seeking a solution in the form of

$$\Psi(x, y, t) = \bar{\Psi}(x, y) + \frac{A}{2} \psi(x, y) e^{it} + O(A^2) + c.c., \tag{6a}$$

$$\Theta(x, y, t) = \bar{\Theta}(x, y) + \frac{A}{2} \theta(x, y) e^{it} + O(A^2) + c.c., \tag{6b}$$

where $\bar{\Psi}, \bar{\Theta}$ are the underlying steady flow and ‘c.c.’ indicates the complex conjugate. Substitution into (2) results in a linear parabolic problem for the perturbations ψ and θ , which can be marched downstream, subject to the corresponding (linearised) source conditions obtained from (3).

In Fig. 2(a) we show the evolution of the axis perturbation speed $\psi_y(x, y = 0)$ for $Pr = 0.71, G_0 = 1, \gamma = 40$ and $S = 4, 12$. It is clear that higher frequencies are associated with a more rapid downstream growth and a shorter wavelength; this will be fully described in the far-downstream limit below.

In Fig. 2(b) we show the axis-values of downstream speed $\Psi_y(x, y = 0, t)$ and temperature $\Theta(x, y = 0, t)$ for a nonlinear periodic state of pulsation amplitude of $A = 0.02$ (again $Pr = 0.71, G_0 = 1, \gamma = 40, S = 12$) and $t = 0, \pi/2, \pi, 3\pi/2$. For comparison, also included is the corresponding scaled linear result of $\bar{\Psi}_y(x, y = 0) + 0.02\psi_y(x, y = 0)$ and $\bar{\Theta}(x, y = 0) + 0.02\theta(x, y = 0)$. At a pulsation amplitude of $A = 0.02$ there is agreement between the nonlinear and the scaled linearised solution near to the source. However, further downstream we find a steepening of the propagating wave as nonlinear effects become important, a behaviour that is consistent with that found in the jet flows considered by Hewitt and Duck [5].

2.1.1. A far-downstream description of the wave

As presented by Brand and Lahey [3] a self-similar steady solution exists to (2) that, in the context of the full parabolic problem with arbitrary source profiles, forms a far-downstream limiting state:

$$\bar{\Psi}(x, y) = (x + x_0)^{1-b} G(Y), \tag{7a}$$

$$\bar{\Theta}(x, y) = (x + x_0)^{1-4b} H(Y), \tag{7b}$$

$$Y = \frac{y}{(x + x_0)^b}, \tag{7c}$$

where $x = -x_0$ is a (virtual) origin. The profiles G and H satisfy

$$G''' + H + (1 - b)GG'' + (2b - 1)(G')^2 = 0, \tag{7d}$$

$$H'' + \sigma(1 - b)GH' + \sigma(4b - 1)HG' = 0, \tag{7e}$$

with boundary conditions $G(0) = G'(0) = H'(0) = 0$ and $H(\infty) = G(\infty) = 0$. The exponent b is determined by requiring that the net

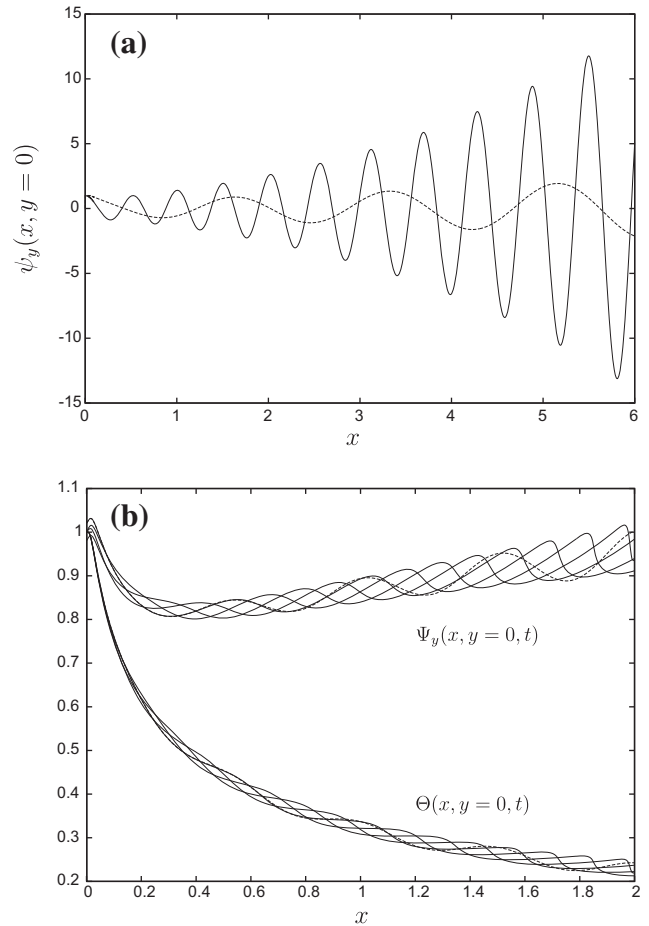


Fig. 2. (a) The downstream centreline velocity of the linearised ($A \ll 1$) perturbation, ψ_y at $y = 0$ as defined by (6), for $G_0 = 1, \sigma = 0.71, \gamma = 40$ at $S = 4$ (dashed) and $S = 12$ (solid). (b) The corresponding nonlinear periodic solution for a pulsation amplitude $A = 0.02$ and $S = 12$, evaluated along the centerline $y = 0$, when $t = 0, \pi/2, \pi, 3\pi/2$ (solid). A scaled linear result is shown as the dashed line to highlight the nonlinear downstream wave steepening.

downstream heat flux (4) is independent of the downstream position, giving

$$b = \frac{2}{5}. \tag{7f}$$

In (7), the functional forms G and H are to be determined such that the integral (4) matches the known source heat flux imposed at $x = 0$. To satisfy the integral constraint, we note that the equations governing G and H are invariant under the transformation

$$G \rightarrow CG, \quad H \rightarrow C^4H, \quad Y \rightarrow Y/C. \tag{8}$$

This allows us to specify an arbitrary non-zero amplitude for G or H , then an appropriate value of C can be determined from an evaluation of (4) using the known source conditions at $x = 0$.

Given this far-downstream steady self-similar base flow, we can now provide an asymptotic description of the downstream development of small-amplitude unsteadiness. To achieve this we use the similarity solution (7) in the expansion (6), after which it is convenient to rewrite:

$$\psi(x, y) = (x + x_0)^{1-b} f(X, Y), \tag{9a}$$

$$\theta(x, y) = (x + x_0)^{1-4b} h(X, Y), \tag{9b}$$

$$X = (x + x_0)^{2b}, \tag{9c}$$

where Y is defined in (7). The linear perturbation equations are then (on replacing $b = 2/5$ for the plume scaling)

$$3(fG)_{YY} - 8f_Y G' + 5f_{YY} + 5h + X(-5iSf_Y + 4(G''f_X - G'f_{XY})) = 0 \tag{10a}$$

and

$$3(hG)_{YY} + 3(fH)_{YY} - 6f_Y H' - 6h_Y G' + 5h_{YY} + X(-5iSh + 4(H'f_X - G'h_X)) = 0, \tag{10b}$$

subject to $f(Y=0) = f_{YY}(Y=0) = h_Y(Y=0) = f_Y(Y \rightarrow \infty) = h(Y \rightarrow \infty) = 0$.

We do not repeat the analysis of [5] here, but simply note that one can obtain a locally wave-like solution for the perturbation (f, h) in an outer, $Y = O(1)$, region as $X \rightarrow \infty$ by balancing the terms proportional to X in (10):

$$f(X, Y) = (f_0(Y) + \dots) \exp(-iKX + a_2 X^{1/2} + a_3 \log X + \dots), \tag{11a}$$

$$h(X, Y) = (h_0(Y) + \dots) \exp(-iKX + a_2 X^{1/2} + a_3 \log X + \dots), \tag{11b}$$

where, $K = 5S/4G'(0)$ is a local wavenumber, and $a_{2,3}$ are constants to be found, with

$$f_0(Y) = G'(Y) - G'(0), \quad h_0(Y) = H'(Y). \tag{11c}$$

This wavenumber K corresponds to a leading order phase speed that matches the axial velocity of the underlying jet/plume.

This outer solution does not satisfy all the required conditions on $Y = 0$, and this is rectified in an inner viscous critical layer that also determines the factor a_2 , the real part of which determines the downstream spatial growth. In this layer, a balance of (10) reintroduces the viscous term f_{YY} when $Y = O(X^{-1/4})$ as discussed in both [6,5]. Despite this system being a plume, rather than a jet, the analysis still follows that given in the appendix of [5], because the buoyancy term h in (10a) remains too small to enter into the analysis for a_2 . However, the thermal nature of the plume does still play a role in the downstream growth via the base flow properties. The result (A8) of Hewitt and Duck [5] can be rewritten as

$$a_2 = \sqrt{iS} \left(\frac{-G'''(0)}{2b^2 G'(0)^3} \right)^{1/2}, \tag{12}$$

on recognising that for a planar jet flow $G'''(0) + (2b-1)G'(0)^2 = 0$. For a planar plume as discussed here, evaluation of (7d) at the axis of symmetry shows that $G'''(0) + H(0) + (2b-$

$1)G'(0)^2 = 0$, and the downstream spatial growth (12) is now modified slightly to be

$$a_2 = \sqrt{iS} \left(\frac{H(0) + (2b-1)G'(0)^2}{2b^2 G'(0)^3} \right)^{1/2}. \tag{13}$$

The temperature of the plume, its associated heat flux, the source (scaled) Grashof number and the Prandtl number will all influence this growth rate through the base flow quantities $H(0)$ and $G'(0)$.

In conclusion, linearised harmonic perturbations to the base plume flow are predicted to grow downstream in agreement with our numerical results. For a perturbation of the form (6), if we consider the magnitude of a periodic perturbation to the plume velocity at the axis, u_c say, then our asymptotic theory predicts

$$u_c(x) = |\psi_y(x, 0)| \sim B(x + x_0)^d \exp(a_{2r}(x + x_0)^b) \tag{14}$$

for large x , where a_{2r} is the real part of (13), B is an amplitude constant and d is a higher order algebraic attenuation coefficient related to a_3 in (11). We do not determine d here, it is only found at higher order in the expansion for large X .

Given the predicted form of (14), a quantitative comparison can be made to our linearised numerical results. Fig. 3(a) demonstrates that the far-field steady solutions (in the absence of pulsation: $A = 0$) are in agreement with the associated self-similar solutions (7). To validate the downstream growth observed in a linear perturbation to this steady base flow, we compute the quantity

$$b^{-1}(x + x_0)^{(1-b)} \frac{u'_c(x)}{u_c(x)} = a_{2r} + O((x + x_0)^{-b}), \tag{15}$$

which for large x is predicted to asymptote to a_{2r} , the real part of (13). The numerical results of Fig. 3(b) are in agreement with this asymptotic description both in the qualitatively observed downstream growth, and the quantitative exponential growth coefficient.

3. Discussion

The evolution of an unsteady laminar plume, modelled by the two-dimensional boundary-layer equations, has been re-examined by a combination of numerical solutions and an asymptotic description far downstream. It is found that any unsteady pulsation of the source conditions leads to a downstream growing wave, in contradiction to the numerical results of Marzouk et al. [4], in

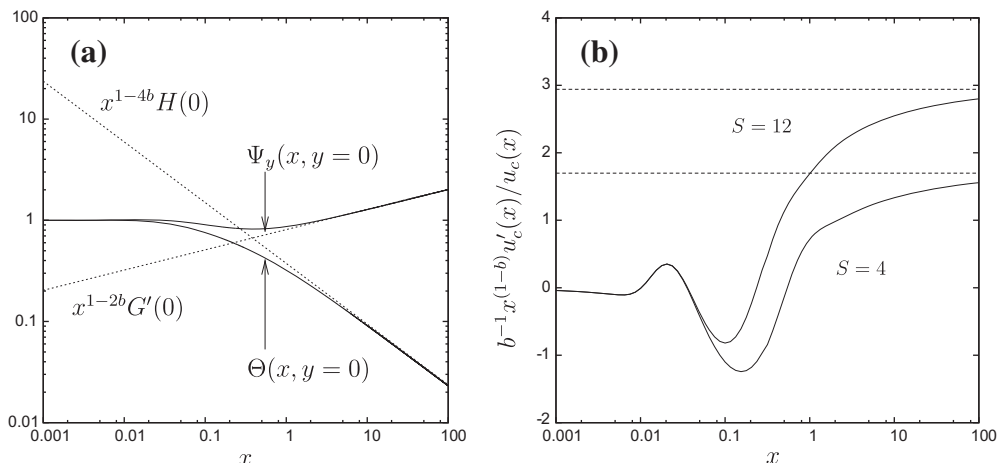


Fig. 3. (a) The downstream evolution of the centreline velocity of the steady base flow $\Psi_y(x, y = 0)$ and the centreline temperature $\Theta(x, y = 0)$. Also shown is the far-downstream asymptotic prediction (7) (dashed lines). (b) The downstream growth metric (15) for $S = 4$ and $S = 12$, as determined from the linearised numerical results (solid lines), compared to the asymptotic ($x \gg 1$) predictions of a_{2r} as obtained from (13) (dashed lines). Both (a) and (b) use parameters $G_0 = 1$, $\sigma = 0.71$, $\gamma = 40$, and comparisons are made with a virtual origin of $x_0 = 0$, which avoids any fitting to the data.

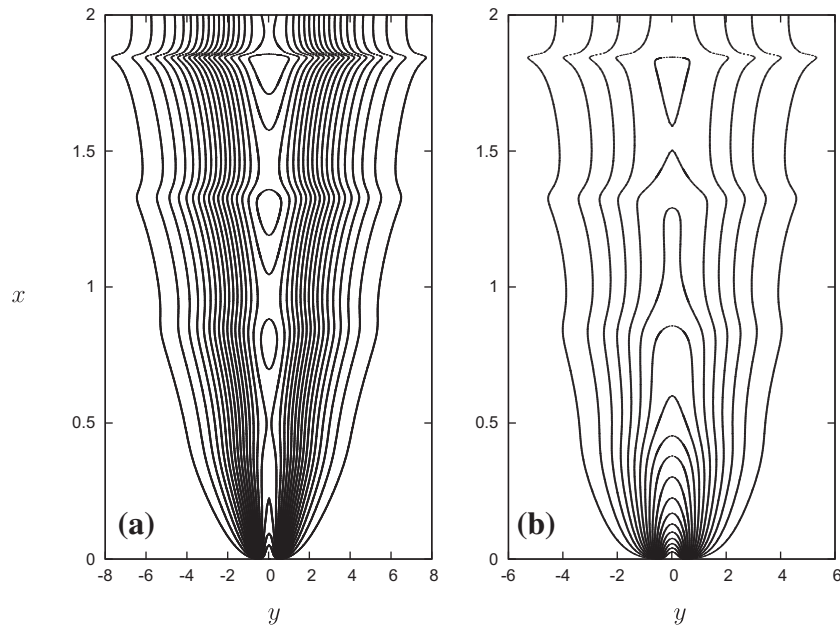


Fig. 4. Contours of (a) streamwise plume velocity $\Psi_y(x, y, t)$ and (b) $\Theta(x, y, t)$ for a periodic pulsatile state, with $A = 0.02$ and $t = 3\pi/2$. Here $G_0 = 1$, $\gamma = 40$, $\sigma = 0.71$ and $S = 12$. Contours levels are shown in increments of 0.05, starting at 0.05.

which the unsteady perturbation decayed. Our nonlinear numerical results are validated against a linearised description in the limit of small amplitude pulsation of the source conditions. The linearised numerical results are in turn validated against an analytic asymptotic description far from the source.

Our linearised theory can be constructed far from the source, because in this region the underlying steady plume is self similar, which allows for an analogous description of the superposed oscillations. This analytical description predicts that (locally) the perturbation is a wave of wavelength proportional to $(x + x_0)^{1/5}$, which remains short compared to the $(x + x_0)^{2/5}$ downstream thickening of the plume. In the linear regime ($A \ll 1$) the induced wave propagates at the same speed as the underlying base flow at leading order. However, the downstream propagation of the wave is accompanied by spatial growth proportional to (in dimensional terms)

$$\left(\frac{x^*}{Re h}\right)^d \exp\left[a_{2r} S^{1/2} Re^{-3/5} \left(\frac{x^*}{h}\right)^{2/5}\right], \quad (16)$$

where we leave d undetermined and a_{2r} is given by (13); this can be compared to the result (1) obtained in the absence of buoyant forcing.

A notable feature of (16) is that the spatial growth is proportional to $S^{1/2}$, which is the dimensionless frequency of oscillation. Even in the ideal case of a single-frequency pulsation, quadratic nonlinearity of the full boundary-layer system will still cause a cascade to higher frequencies that grow ever more rapidly downstream. This subtle effect was shown in Hewitt and Duck [5] to lead to a breakdown of the boundary-layer equations at a finite distance downstream from the source, a point at which the assumption that the flow develops over a long downstream length scale of $O(Re h)$ fails; h being the width of the flow at its source. The same features exist in this plume case and we do not repeat them in detail, but Fig. 4 shows contours of streamwise plume velocity and temperature for the same periodic state shown in Fig. 2(b). The growth of pulsations is clearly seen, as is the wave steepening. Eventually a breakdown of the boundary layer system is obtained in the manner described by [5] at a critical value of x ,

indicating the existence of $O(h)$ downstream length scales and a loss of the boundary-layer approximation.

These (inflectional) flows are known to be unstable to inviscid modes of downstream wavelength $O(h)$, so the downstream development of the flow is crucially dependent on the amplitude and frequency spectrum of any noise present in the system. However, the mechanism discussed herein is best viewed as being a process able to amplify small scale high-frequencies through a combination of spatial growth and nonlinear interaction, which can then feed into inviscid instabilities (at the critical downstream position). Furthermore, although we have focussed exclusively on laminar plumes in this discussion, we may also note that the classical integrated (turbulent) plume model of Morton et al. [9] suffers from an analogous downstream growth when extended to unsteady source conditions (as do other similar turbulent plume models), as recently demonstrated by Scase and Hewitt [10]. This is perhaps surprising, given that the turbulent integrated model removes all detail of the flow profile, but the qualitative similarities are striking and further work is warranted on other comparable models of turbulent jets/plumes and their response to pulsation of source conditions.

References

- [1] v.H. Schlichting, Laminare strahlbreitung, ZAMM – J. Appl. Math. Mech./Z. Angew. Math. Mech. 13 (1933) 260–263.
- [2] W. Bickley, The plane jet, Philos. Mag. 23 (1937) 727–731.
- [3] R. Brand, F. Lahey, The heated laminar vertical jet, J. Fluid Mech. 29 (1967) 305–315.
- [4] S. Marzouk, H. Mhiri, S. El Golli, G. Le Palec, P. Bournot, Numerical study of momentum and heat transfer in a pulsed plane laminar jet, Int. J. Heat Mass Transfer 46 (2003) 4319–4334.
- [5] R. Hewitt, P. Duck, Pulsatile jets, J. Fluid Mech. 670 (2011) 240–259.
- [6] N. Riley, M. Sánchez-Sanz, E. Watson, A planar pulsating jet, J. Fluid Mech. 638 (2009) 161.
- [7] S. Cowley, L. Hocking, O. Tutty, The stability of solutions of the classical unsteady boundary-layer equation, Phys. Fluids 28 (1985) 441.
- [8] H. Keller, Numerical methods in boundary-layer theory, Ann. Rev. Fluid Mech. 10 (1978) 417–433.
- [9] B. Morton, G. Taylor, J. Turner, Turbulent gravitational convection from maintained and instantaneous sources, Proc. R. Soc. London. Ser. A. Math. Phys. Sci. 234 (1956) 1–23.
- [10] M. Scase, R. Hewitt, Unsteady turbulent plume models, J. Fluid Mech. 697 (2012) 455–480.